coatings

MDPI

Article

Exchange Bias Effect in $LaFeO_3$: $La_{0.7}Ca_{0.3}MnO_3$ Composite Thin Films

Feng Wang [1,†], Wei Fu [2,†], Chengming Jiang [3], Junxiao Li [4,*] and Jijie Huang [5,*]

1 Department of Vehicle Engineering, Changzhou Vocational Institute of Mechatronic Technology, Changzhou 213164, China; wangfeng322@163.com
2 Qingdao Special Service Sanatorium of PLA Navy, Qingdao 266000, China; Izzie.11@163.com
3 Key Laboratory for Precision and Non-Traditional Machining Technology of the Ministry of Education, Dalian University of Technology, Dalian 116024, China; jiangcm@dlut.edu.cn
4 Institute of Oceanographic Instrumentation, Qilu University of Technology (Shandong Academy of Science), Qingdao 266001, China
5 School of Materials, Sun Yat-sen University, Guangzhou 510275, China
* Correspondence: lijunxiao521@qlu.edu.cn (J.L.); huangjj83@mail.sysu.edu.cn (J.H.)
† These authors contribute equally to this work.

Abstract: Composite thin films arouse great interests owing to the multifunctionalities and heterointerface induced physical property tailoring. The exchange bias effect aroused from the ferromagnetic (FM)–antiferromagnetic (AFM) heterointerface is applicable in various applications such as magnetic storage. In this work, $(LaFeO_3)_x$:$(La_{0.7}Ca_{0.3}MnO_3)_{1-x}$ composite thin films have been deposited via pulsed laser deposition (PLD) and the exchange bias effect was investigated. In such system, $LaFeO_3$ (LFO) is an antiferromagnet while $La_{0.7}Ca_{0.3}MnO_3$ (LCMO) is a ferromagnet, which results in the exchange bias interfacial coupling at the FM/AFM interface. The composition variation of the two phases could lead to the exchange bias field (H_{EB}) tuning in the composite system. This work demonstrates a new composite thin film system with FM-AFM interfacial exchange coupling, which could be applied in various spintronic applications.

Keywords: exchange bias; composite thin film; magnetic property; heterointerface

Citation: Wang, F.; Fu, W.; Jiang, C.; Li, J.; Huang, J. Exchange Bias Effect in $LaFeO_3$: $La_{0.7}Ca_{0.3}MnO_3$ Composite Thin Films. *Coatings* **2021**, *11*, 1125. https://doi.org/10.3390/coatings11091125

Academic Editor: Gianni Barucca

Received: 31 August 2021
Accepted: 10 September 2021
Published: 16 September 2021

1. Introduction

Exchange bias (EB) describes the pinning of the magnetic dipoles due to the interfacial exchange coupling between ferromagnetic (ferrimagnetic, FM) and antiferromagnetic (AFM) components after cooling through Néel temperature (T_N) of the antiferromagnets, which results in the shift of the hysteresis loop. The EB field (H_{EB}) is used to evaluate the EB effect, which could be defined as $H_{EB} = |H_+ + H_-|/2$, where H_+ and H_- are the positive and negative coercivity in the hysteresis loop, respectively. The EB phenomenon was first observed in the AFM CoO nanoparticle wrapped by an FM Co shell, reported by Meiklejohn and Bean in 1956, and the Meiklejohn–Bean model has been widely accepted to explain the mechanism of EB effect [1]. The EB effect could be employed in a lot of applications, such as magnetoresistive read heads, magnetic sensors, spin valve devices, as well as high-density data storage [2–5]. Thus far, the EB effect has been realized in various material systems and geometries, such as granular composites, core–shell nanoparticles, nanocluster arrays with capping layer and thin films [6–9].

Among all the different nanostructures with EB effect, the thin film form might be the most promising for practical applications, and a tremendous research effort has been devoted to exploring the EB effect in thin films. Typically, the FM/AFM exchange coupling in thin film could be achieved in the following forms: multilayer thin film, vertically aligned nanocomposite thin film, solid solution (or composite) thin film or even a single-phase thin film [10–13]. Multilayer is the most conventional approach to obtain the EB effect, which alternatively grows FM and AFM layers to create a transverse FM/AFM

interface. The multilayers could be stacked by different material combinations, such as metal/alloy, metal/oxide and oxide/oxide, for example. Co/CuMn bilayer, Fe/FeO bilayer and $La_{0.7}Sr_{0.3}MnO_3$ (LSMO)/$BiFeO_3$ (BFO) bilayer have been designed to investigate their EB effect [14–16]. The H_{EB} could be tailored by tuning the number of layer and the thickness of each layer, for example, the relationship between H_{EB} and the thickness of the FM layer (t_{FM}) is derived as $H_{EB} \propto 1/t_{FM}$ [17]. The composite thin film evolving FM and AFM components is another platform to achieve EB, which forms a unique nanostructure of one phase exhibited as nanopillars embedding into another matrix phase, termed as vertically aligned nanocomposite (VAN) thin film. Different from the transverse FM/AFM interface in multilayers, VAN thin film presents FM/AFM coupling along the vertical direction, which is beneficial to realize perpendicular EB effect. Various oxide systems have been explored, such as LSMO:NiO, LSMO:$LaFeO_3$ (LFO), NiO:$NiFe_2O_4$ (NFO), BFO:Fe_3O_4, etc. [18–22]. Similar lattice parameters/crystal structures and phase immiscibility are required to form such VAN structure, otherwise it is highly possible to be phase mixed as a solid solution or composite thin film. Solid solution thin films with FM and AFM phases can also induce the EB effect by the FM/AFM exchange coupling in nanoscale interface [12]. Lastly, the EB effect has been observed even in single-phase thin films, which is induced by either defects [23], strain [24] or some unusual interfaces [13,25]. Overall, although the EB effect has been obtained in variety of thin films with different nanostructures, there are still plenty of material systems and geometries needing further investigation.

In this work, a new FM-AFM system has been developed for the EB effect, e.g., LFO and $La_{0.7}Ca_{0.3}MnO_3$ (LCMO) are selected as the AFM phase and FM phase, respectively. We deposited LFO_x:$LCMO_{1-x}$ (x = 0.33, 0.5, 0.67) composite thin films by pulsed laser deposition (PLD) and investigated their EB effect; the thickness of the films was controlled at ~200 nm. Both LFO (a = 3.940 Å, pseudo-cubic) and LCMO (a = 3.867 Å, pseudo-cubic) present perovskite structures with lattice parameters close to the selected STO (001) substrate (a = 3.905 Å, cubic). LFO is a typical AFM material (T_N = 710 K) and has been applied in various systems with an EB effect [19,26,27], while LCMO is a widely studied FM material (Curie temperature T_C = 225 K). [28] Therefore, the EB effect is expected in the LFO:LCMO composite thin film, and the H_{EB} value can be tailored by varying the composition of the two phases.

2. Materials and Methods

Target Preparation and Thin Film Deposition: LFO_x:$LCMO_{1-x}$ (x = 0.33, 0.5, 0.67) targets were made by a conventional solid-state mixing of the LFO and LCMO powders with the designed ratio, high-pressure pressing into a 1-inch pellet and followed by a sintering process at 1200 °C for 10 h. Then, the thin films were deposited using a pulsed laser deposition (PLD) system with a KrF excimer laser (Lambda Physik, λ = 248 nm). The detailed deposition parameters are as follows: base pressure was below 1×10^{-6} Torr, 45 Pa of high-purity O_2 was inflowed into the chamber during deposition, the deposition temperature was 750 °C, the deposition frequency was 5 Hz, target-substrate distance was 4.5 cm and laser energy was 1 mJ/cm^2; after deposition, 30 kPa O_2 was inflowed into the chamber and the samples were cooled down at 10 °C/min.

Microstructure Characterizations: The crystal structure of the films was characterized by X-ray diffraction (XRD) (Panalytical X'Pert X-ray diffractometer). The surface morphology of the films was characterized by atomic force microscopy (AFM, Bruker Icon AFM).

Physical Property Characterizations: Temperature dependence of ZFC and FC magnetization (M-T, 5-380 K) and magnetic hysteresis curves (M-H, field along the direction perpendicular to the film surface) were carried out by using a vibrating sample magnetometer (VSM) in the physical property measurement system (PPMS: Quantum Design).

3. Results and Discussion

The main aspect of this work is to grow a new FM-AFM system with a tunable EB effect by composition variation of the two phases. First, standard θ–2θ XRD scans were characterized on the LFO:LCMO thin films with different compositions, as shown in Figure 1a–c for $LFO_{0.33}LCMO_{0.67}$, $LFO_{0.5}LCMO_{0.5}$ and $LFO_{0.67}LCMO_{0.33}$, respectively. Only LFO (00l) and LCMO (00l) peaks can be observed, which indicates the textured growth of both phases and that no impurity is formed in the composite films (note that the peak at ~42° is from the instrument, not from the samples). To obtain the actual 2θ values of the LFO (002) and LCMO (002) peaks, the local area (45–48°) has been enlarged and shown in the right panels of Figure 1. The 2θ values of the LFO (002) and LCMO (002) peaks can be identified as 46.285° and 46.607°, which corresponds to the $d_{(001)}$ values of 3.921 Å and 3.895 Å for LFO and LCMO, respectively. Compared to the bulk values, the LFO phase and LCMO phases in the composite thin film undergo out-of-plane compressive strain of −0.48% and tensile strain of 0.72%, respectively.

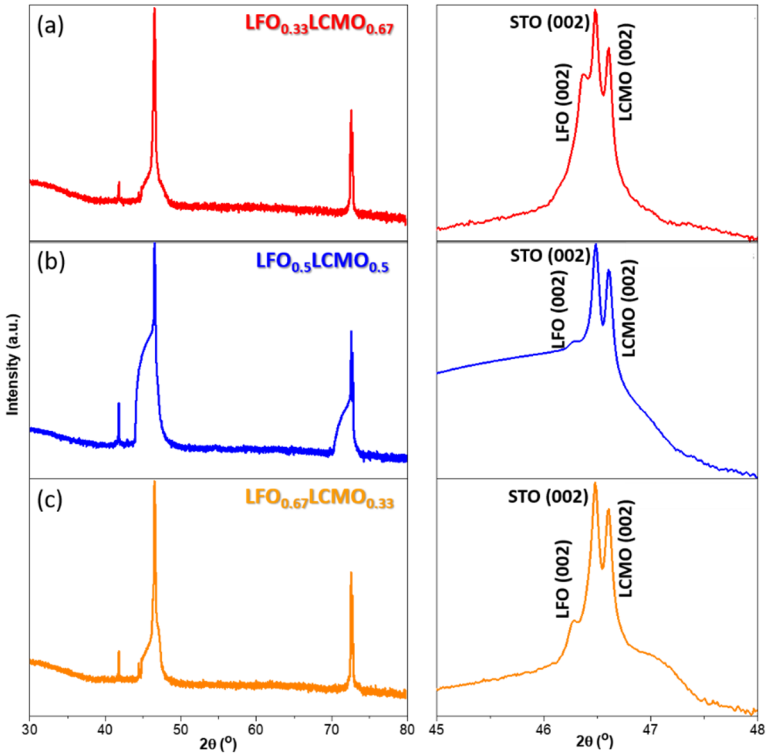

Figure 1. Standard θ–2θ XRD scans on LFO:LCMO thin films with different compositions. (**a**) $LFO_{0.33}LCMO_{0.67}$; (**b**) $LFO_{0.5}LCMO_{0.5}$ and (**c**) $LFO_{0.67}LCMO_{0.33}$. The right panels are the local scan from 45° to 48°.

An atomic force microscope (AFM) has been used to investigate the surface morphology of the composite thin films, and the AFM images with 2 μm × 2 μm squares are shown in Figure 2a–c for $LFO_{0.33}LCMO_{0.67}$, $LFO_{0.5}LCMO_{0.5}$ and $LFO_{0.67}LCMO_{0.33}$ composite thin films, respectively. As is shown, $LFO_{0.33}LCMO_{0.67}$ presents a relatively rough surface with large domains, and the surface roughness (R_a) was determine to be 4.97 nm. On another side, $LFO_{0.5}LCMO_{0.5}$ and $LFO_{0.67}LCMO_{0.33}$ films exhibit a very smooth surface with R_a of 0.554 nm and 0.793 nm, and the domains are relatively small. It is highly possible that the neighboring domains are the FM and AFM phases; thus, the FM/AFM interfacial coupling occurs at the domain boundaries.

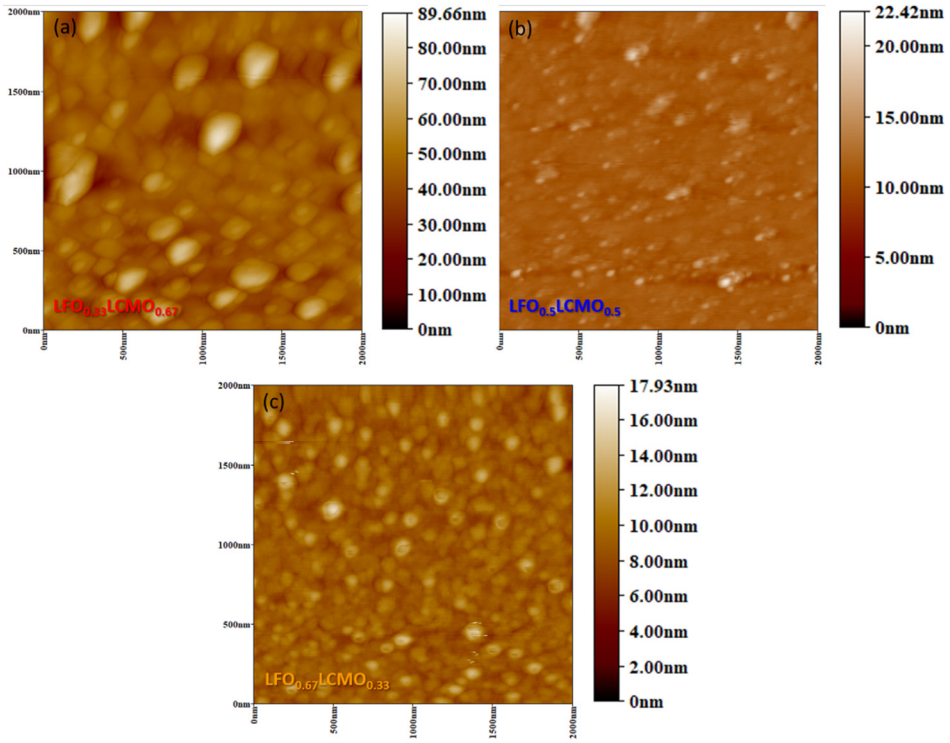

Figure 2. Atomic force microscopic images to show the surface morphology of (**a**) $LFO_{0.33}LCMO_{0.67}$, (**b**) $LFO_{0.5}LCMO_{0.5}$ and (**c**) $LFO_{0.67}LCMO_{0.33}$ composite thin films.

Then, the magnetization hysteresis (M-H) loops of all the samples were measured at different temperatures (10 K, 50 K, 150 K, 250 K and 300 K). The M-H loops of the $LFO_{0.67}LCMO_{0.33}$ film are shown in Figure 3a–d for 10 K, 50 K, 150 K and 250 K measurements; all of the loops exhibit typical M-H curves for hard magnets. An obvious EB effect can be identified, as a difference has been observed between the positive and negative coercivity. Another interesting feature is that the M-H curves are not smoothly presented; multiple steps can be observed, especially close to the saturation point that might result from the multiple magnetic components in the system, such as the FM LCMO phase, AFM LFO phase and the FM/AFM interface. The $LFO_{0.33}LCMO_{0.67}$ and $LFO_{0.5}LCMO_{0.5}$ samples exhibit similar shapes of the M-H loops with varying saturation magnetization (M_s) and coercivity (H_c) values (data not shown here).

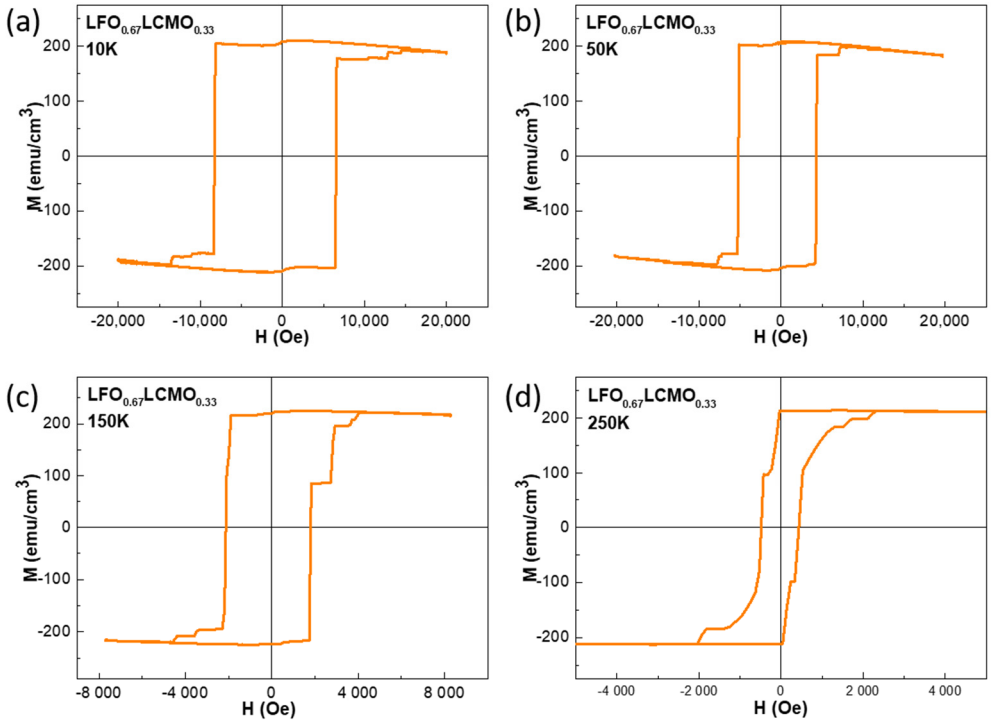

Figure 3. The magnetization hysteresis (M-H) loops of the $LFO_{0.67}LCMO_{0.33}$ film measured at (**a**) 10 K, (**b**) 50 K, (**c**) 150 K and (**d**) 250 K.

Based on the M-H curves, the EB field ($H_{EB} = |H_+ + H_-|/2$), coercivity ($H_C = |H_+ + H_-|/2$) and M_s values at different temperatures can be estimated and all the data for different samples are shown and compared in Figure 4a–c, respectively. When the temperature increases, the H_{EB} and H_C values decreases, which is a normal phenomenon in an AFM/FM system. Among the three samples with different composition, the $LFO_{0.67}LCMO_{0.33}$ film obtains the highest H_{EB} and H_C values at all the measured temperatures. The H_{EB} values are 891 Oe, 459 Oe, 162 Oe and 28 Oe at 10 K, 50 K, 150 K and 250 K, respectively, and it diminishes at 300 K. The M_s values at different temperatures of all the samples are also compared in Figure 4c. The M_s values increase with a higher LCMO phase in the composite film as the FM LCMO has a much stronger magnetic response than the AFM LFO phase.

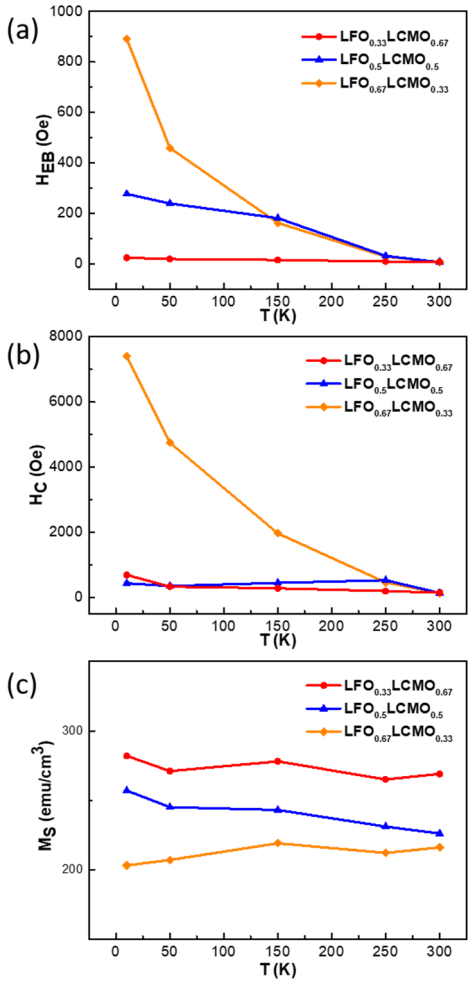

Figure 4. Magnetic properties comparison of the composite thin films with different compositions, which are (**a**) H_{EB} value, (**b**) H_C value and (**c**) M_s value.

To further explore the magnetic properties of the composite thin film system, temperature dependence of zero-field cooling (ZFC) and field cooling (FC, 1000 Oe) magnetization (M-T) measurements of all the samples with different compositions have been carried out and compared in Figure 5. All the samples show a similar trend. For the FC condition, the magnetization decreases with increasing temperature (10−350 K) monotonically. However, for ZFC condition, magnetization firstly increases to a maximum value (blocking temperature: T_B) and then decreases with increasing temperature. Another feature is the bifurcation between the ZFC and FC curves, which could be used to define the irreversibility temperature (T_{irr}). The T_B value is slightly lower than T_{irr}, which has been observed in many other magnetic systems [29,30]. Overall, the LFO:LCMO composite thin films presents an interesting magnetic response; specifically, the large H_{EB} values demonstrate a strong exchange interfacial coupling between the AFM LFO phase and FM LCMO phase. This new FM-AFM design provides more insights into how to develop composite thin films with the EB effect, and how to tune and optimize the H_{EB} values via deposition condition optimization and composition variation to generate different nanostructures.

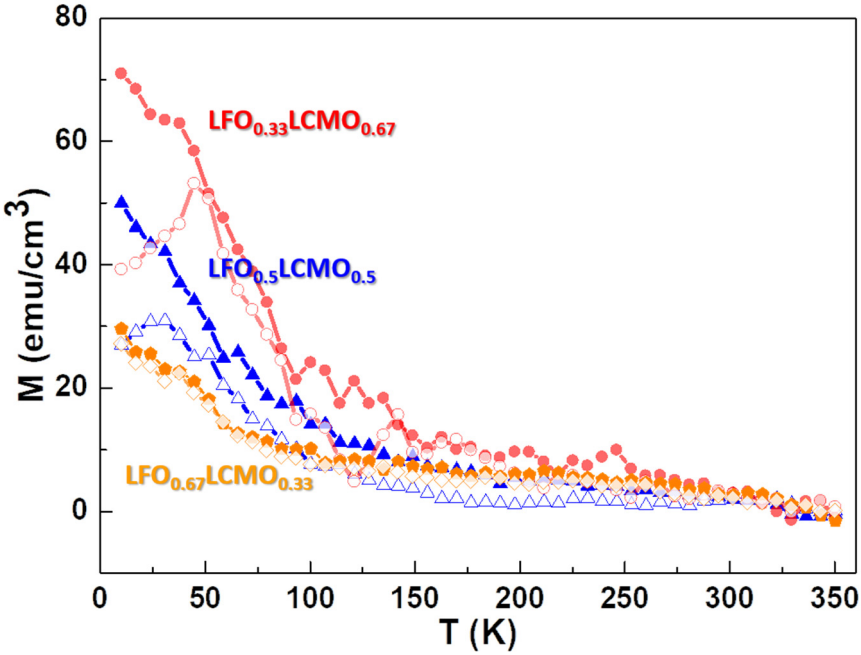

Figure 5. Temperature dependence of zero-field cooling (ZFC, solid symbols) and field cooling (FC, 1000 Oe, hollow symbols) magnetization of all the samples with different compositions.

4. Conclusions

A new composite thin film system of LFO:LCMO with different compositions has been grown and characterized in order to achieve a tailorable exchange bias effect by composition variation. The composite thin films show excellent crystal quality with c-axis growth for both the LFO and LCMO phases. Furthermore, an obvious shift of the hysteresis loops has been observed for all the films, while the $LFO_{0.67}LCMO_{0.33}$ sample obtains the strongest FM-AFM interfacial exchange coupling. The H_{EB} values of such film are estimated as 891 Oe, 459 Oe, 162 Oe and 28 Oe at 10 K, 50 K, 150 K and 250 K, respectively, which is relatively large compared to other oxide–oxide composite thin films. Furthermore, both blocking temperature and irreversibility temperature can be determined from the FC and ZFC M-T measurements.

Author Contributions: Conceptualization, C.J. and J.H.; methodology, F.W. and W.F.; formal analysis, F.W., W.F. and J.L.; investigation, F.W., W.F. and C.J.; resources, J.H.; writing—original draft preparation, F.W. and W.F.; writing—review and editing, C.J., J.L. and J.H.; supervision, J.H.; project administration, J.H.; funding acquisition, J.H. All authors have read and agreed to the published version of the manuscript.

Funding: J.H. acknowledges the support from Guangdong Basic and Applied Basic Research Foundation (2019A1515111029) and the Fundamental Research Funds for the Central Universities (20lgpy13). F.W acknowledges the support from Qing Lan project.

Institutional Review Board Statement: Not applicable.

Informed Consent Statement: Not applicable.

Data Availability Statement: Data is contained within the article.

Conflicts of Interest: The authors declare no conflict of interest.

References

1. Meiklejohn, W.H.; Bean, C.P. New magnetic anisotropy. *Phys. Rev.* **1956**, *105*, 904–913. [CrossRef]
2. Wei, Z.; Sharma, A.; Nunez, A.S.; Haney, P.M.; Duine, R.A.; Bass, J.; MacDonald, A.H.; Tsoi, M. Changing exchange bias in spin valves with an electric current. *Phys. Rev. Lett.* **2007**, *98*, 116603. [CrossRef] [PubMed]

3. Klug, M.J.; Thormählen, L.; Röbisch, V.; Toxværd, S.D.; Höft, M.; Knöchel, R.; Quandt, E.; Meyners, D.; McCord, J. Antiparallel exchange biased multilayers for low magnetic noise magnetic field sensors. *Appl. Phys. Lett.* **2019**, *114*, 192410. [CrossRef]
4. Tian, Z.; Xu, L.; Gao, Y.; Yuan, S.; Xia, Z. Magnetic memory effect at room temperature in exchange coupled $NiFe_2O_4$-NiO nanogranular system. *Appl. Phys. Lett.* **2017**, *11*, 182406. [CrossRef]
5. Liao, X.; Gao, L.; Wang, Y.; Xu, X.; Khan, M.T.; Chang, T.; Chen, K.; Zeng, Y.; Yang, S.; Svedlindh, P. Large exchange bias in magnetic shape memory alloys by tuning magnetic ground state and magnetic-field history. *Sci. China Mater.* **2020**, *63*, 1291–1299. [CrossRef]
6. Franceschin, G.; Gaudisson, T.; Menguy, N.; Dodrill, B.C.; Yaacoub, N.; Grenèche, J.; Valenzuela, R.; Ammar, S. Exchange-biased $Fe_{3-x}O_4$−CoO granular composites of different morphologies prepared by seed-mediated growth in polyol: From core-shell to multicore embedded structures. *Part. Part. Syst. Charact.* **2018**, *35*, 1800104. [CrossRef]
7. Binns, C.; Qureshi, M.T.; Peddis, D.; Baker, S.H.; Howes, P.B.; Boatwright, A.; Cavill, S.A.; Dhesi, S.S.; Lari, L.; Kröger, R.; et al. Exchange bias in Fe@Cr core-shell nanoparticles. *Nano Lett.* **2013**, *13*, 3334–3339. [CrossRef]
8. Sessi, V.; Hertenberger, S.; Zhang, J.; Schmitz, D.; Gsell, S.; Schreck, M.; Morel, R.; Brenac, A.; Honolka, J.; Kern, K. Exchange bias in reduced dimensions: Cobalt nanocluster arrays under the influence of nanometer thin MnPt capping layers. *J. Appl. Phys.* **2013**, *113*, 123903. [CrossRef]
9. Blachowicz, T.; Ehrmann, A. Exchange bias in thin films-an update. *Coatings* **2021**, *11*, 122. [CrossRef]
10. Maat, S.; Takano, K.; Parkin, S.S.P.; Fullerton, E.E. Perpendicular exchange bias of Co/Pt multilayers. *Phys. Rev. Lett.* **2001**, *87*, 087202. [CrossRef]
11. Huang, J.; Gellatly, A.; Kauffmann, A.; Sun, X.; Wang, H. Exchange bias effect along vertical interfaces in $La_{0.7}Sr_{0.3}MnO_3$:NiO vertically aligned nanocomposite thin films integrated on silicon substrates. *Cryst. Growth Des.* **2018**, *18*, 4388–4394. [CrossRef]
12. Lorenz, M.; Ziese, M.; Wagner, G.; Lenzner, J.; Kranert, C.; Brachwitz, K.; Hochmuth, H.; Esquinazi, P.; Grundmanna, M. Exchange bias and magnetodielectric coupling effects in $ZnFe_2O_4$-$BaTiO_3$ composite thin films. *CrystEngComm* **2012**, *14*, 6477–6486. [CrossRef]
13. Sung, K.D.; Park, Y.A.; Seo, M.S.; Jo, Y.; Hur, N.; Jung, J.H. Observation of intriguing exchange bias in $BiFeO_3$ thin films. *J. Appl. Phys.* **2012**, *112*, 033915. [CrossRef]
14. Ali, M.; Adie, P.; Marrows, C.H.; Greig, D.; Hickey, B.J.; Stamps, R.L. Exchange bias using a spin glass. *Nat. Mater.* **2007**, *6*, 70–75. [CrossRef] [PubMed]
15. Fan, Y.; Smith, K.J.; Lüpke, G.; Hanbicki, A.T.; Goswami, R.; Li, C.H.; Zhao, H.B.; Jonker, B.T. Exchange bias of the interface spin system at the Fe/MgO interface. *Nat. Nanotechnol.* **2013**, *8*, 438–444. [CrossRef]
16. Wu, S.M.; Cybart, S.A.; Yu, P.; Rossell, M.D.; Zhang, J.X.; Ramesh, R.; Dynes, R.C. Reversible electric control of exchange bias in a multiferroic field-effect device. *Nat. Mater.* **2010**, *9*, 756–761. [CrossRef] [PubMed]
17. Leighton, C.; Fitzsimmons, M.R.; Hoffmann, A.; Dura, J.; Majkrzak, C.F.; Lund, M.S.; Schuller, I.K. Thickness-dependent coercive mechanisms in exchange-biased bilayers. *Phys. Rev. B* **2002**, *65*, 064403. [CrossRef]
18. Ning, X.; Wang, Z.; Zhang, Z. Large, temperature-tunable low-field magnetoresistance in $La_{0.7}Sr_{0.3}MnO_3$:NiO nanocomposite films modulated by microstructures. *Adv. Funct. Mater.* **2014**, *24*, 5393–5401. [CrossRef]
19. Fan, M.; Zhang, W.; Jian, J.; Huang, J.; Wang, H. Strong perpendicular exchange bias in epitaxial $La_{0.7}Sr_{0.3}MnO_3$:$LaFeO_3$ nanocomposite thin films. *APL Mater.* **2016**, *4*, 076105. [CrossRef]
20. Huang, J.; Wang, H.; Wang, X.; Gao, X.; Liu, J.; Wang, H. Exchange bias in a $La_{0.67}Sr_{0.33}MnO_3$/NiO heterointerface integrated on a flexible mica substrate. *ACS Appl. Mater. Interfaces* **2020**, *12*, 39920–39925. [CrossRef]
21. Wu, R.; Yun, C.; Wang, X.; Lu, P.; Li, W.; Lin, Y.; Choi, E.; Wang, H.; MacManus-Driscoll, J.L. All-oxide nanocomposites to yield large, tunable perpendicular exchange bias above room temperature. *ACS Appl. Mater. Interfaces* **2018**, *10*, 42593–42602. [CrossRef]
22. Choi, E.; Weal, E.; Bi, Z.; Wang, H.; Kursumovic, A.; Fix, T.; Blamire, M.G.; MacManus-Driscoll, J.L. Strong room temperature exchange bias in self-assembled $BiFeO_3$-Fe_3O_4 nanocomposite heteroepitaxial films. *Appl. Phys. Lett.* **2013**, *102*, 012905. [CrossRef]
23. Wang, C.; Chen, C.; Chang, C.; Tsai, H.; Pandey, P.; Xu, C.; Böttger, R.; Chen, D.; Zeng, Y.; Gao, X.; et al. Defect-induced exchange bias in a single $SrRuO_3$ layer. *ACS Appl. Mater. Interfaces* **2018**, *10*, 27472–27476. [CrossRef]
24. Zhou, G.; Ji, H.; Bai, Y.; Quan, Z.; Xu, X. Intrinsic exchange bias effect in strain-engineered single antiferromagnetic $LaMnO_3$ films. *Sci. China Mater.* **2019**, *62*, 1046–1052. [CrossRef]
25. West, K.G.; Nam, D.N.H.; Lu, J.W.; Bassim, N.D.; Picard, Y.N.; Stroud, R.M.; Wolf, S.A. Exchange bias in a single phase ferrimagnet. *J. Appl. Phys.* **2010**, *107*, 113915. [CrossRef]
26. Scholl, A. Domain-size-dependent exchange bias in Co/$LaFeO_3$. *Appl. Phys. Lett.* **2004**, *85*, 4085. [CrossRef]
27. Mohamed, A.A.; Álvarez-Alonso, P.; Hernando, B. The intrinsic exchange bias effect in the $LaMnO_3$ and $LaFeO_3$ compounds. *J. Alloys Compd.* **2021**, *850*, 156713. [CrossRef]
28. Nurgaliev, T.; Topal, U.; Blagoev, B.; Mateev, E. Magnetic properties of LCMO/LSMO thin films on LAO and ALO substrates. *J. Supercond. Nov. Magn.* **2012**, *25*, 2495–2498. [CrossRef]
29. Alonso, J.; Fdez-Gubieda, M.L.; Barandiarán, J.M.; Svalov, A.; Fernández Barquín, L.; Venero, D.A.; Orue, I. Crossover from superspin glass to superferromagnet in Fe_xAg_{100-x} nanostructured thin films ($20 \leq x \leq 50$). *Phys. Rev. B* **2010**, *82*, 054406. [CrossRef]
30. Huang, X.H.; Ding, J.F.; Jiang, Z.L.; Yin, Y.W.; Yu, Q.X.; Li, X.G. Dynamic properties of cluster glass in $La_{0.25}Ca_{0.75}MnO_3$ nanoparticles. *J. Appl. Phys.* **2009**, *106*, 083904. [CrossRef]